doi:10.1016/j.jmb.2006.09.069 J. Mol. Biol. (2007) 365, 649–662

JMB

Available online at www.sciencedirect.com

ScienceDirect

ELSEVIER

Mechanism of Intracellular Block of the KcsA K^+ Channel by Tetrabutylammonium: Insights from X-ray Crystallography, Electrophysiology and Replica-exchange Molecular Dynamics Simulations

José D. Faraldo-Gómez[1]†, Esin Kutluay[2]†, Vishwanath Jogini[3]† Yanxiang Zhao[3], Lise Heginbotham[2] and Benoît Roux[1]*

[1]*Institute for Molecular Pediatric Sciences and Department of Biochemistry and Molecular Biology, University of Chicago, Gordon Center for Integrative Sciences 929 East 57th Street Chicago, IL 60637, USA*

[2]*Department of Molecular Biophysics and Biochemistry Yale University, 266 Whitney Avenue, New Haven, CT 06520 USA*

[3]*Department of Physiology and Biophysics, Training Program in Chemical Biology, Weill Medical College of Cornell University 1300 York Avenue, New York NY 10021, USA*

**Corresponding author*

The mechanism of intracellular blockade of the KcsA potassium channel by tetrabutylammonium (TBA) is investigated through functional, structural and computational studies. Using planar-membrane electrophysiological recordings, we characterize the binding kinetics as well as the dependence on the transmembrane voltage and the concentration of the blocker. It is found that the apparent affinity of the complex is significantly greater than that of any of the eukaryotic K^+ channels studied previously, and that the off-rate increases with the applied transmembrane voltage. In addition, we report a crystal structure of the KcsA–TBA complex at 2.9 Å resolution, with TBA bound inside the large hydrophobic cavity located at the center of the channel, consistent with the results of previous functional and structural studies. Of particular interest is the observation that the presence of TBA has a negligible effect on the channel structure and on the position of the potassium ions occupying the selectivity filter. Inspection of the electron density corresponding to TBA suggests that the ligand may adopt more than one conformation in the complex, though the moderate resolution of the data precludes a definitive interpretation on the basis of the crystallographic refinement methods alone. To provide a rationale for these observations, we carry out an extensive conformational sampling of an atomic model of TBA bound in the central cavity of KcsA, using the Hamiltonian replica-exchange molecular dynamics simulation method. Comparison of the simulated and experimental density maps indicates that the latter does reflect at least two distinct binding orientations of TBA. The simulations show also that the relative population of these binding modes is dependent on the ion configuration occupying the selectivity filter, thus providing a clue to the nature of the voltage-dependence of the binding kinetics.

Keywords: Cation; solvation; binding; hydrophobic; molecular dynamics

Introduction

Small molecules that block the passage of ions across biological channels are one of the most useful tools in electrophysiology for probing the pore-forming regions of these proteins, as well as their gating mechanisms.[1] For example, calcium-activated IKCa1 channels are blocked by TRAM-34,[2] HERG1 is blocked by MK-499,[3] and voltage-gated channels are blocked by bupivacaine.[4] Many such blockers have been identified, and substantial progress has been made towards the characterization of

Present address: Y. Zhao, Hong Kong Polytechnic University, Hong Kong, China.

† J.D.F.-G., E.K. and V.J. contributed equally to this work.

Abbreviations used: QA, quaternary ammonium; TBA, tetrabutylammonium; HREMD, Hamiltonian replica-exchange molecular dynamics.

E-mail address of the corresponding author: roux@uchicago.edu

0022-2836/$ - see front matter © 2006 Published by Elsevier Ltd.

their binding mechanisms; for instance, through point-mutation,[4–6] X-ray crystallography,[7,8] and modeling studies.[9–11] Nonetheless, a deeper understanding of the structural and energetic determinants of these binding processes is of great interest, both to help interpret and design electrophysiological measurements, and to guide the rational design of more selective and potent blockers that may have therapeutic use against diseases such as epilepsy, arrhythmia and long QT syndrome.[12,13]

Arguably, the most extensively used of the ion-channel blockers are the quaternary ammonium (QA) compounds,[14–18] such as tetrabutylammonium (TBA). These cationic compounds access the pore of K^+ channels, primarily from the intracellular side of the membrane, where they are believed to bind by virtue of energetically favorable interactions with the protein, thus blocking the passage of ions directly. The bacterial K^+ channel protein KcsA from *Streptomyces lividians* currently serves as the principal model of the pore domain of potassium channels, since this is the only channel that has been well characterized both electrophysiologically and structurally,[19–23] and has been the subject of in-depth theoretical analyses.[24–28] In addition, KcsA has a relatively high sequence similarity to other K^+ channels, especially in the pore-lining region.[29,30] Hence, KcsA is also a suitable model system to investigate in molecular detail the process of binding of QA blockers to K^+ channels, as illustrated by recent analyses of tetraethylammonium blockade.[8,31]

Here, we aim to further our understanding of the mechanism of blockage of K^+ channels by small compounds such as QA ions, through structural and functional studies of KcsA in association with TBA. Specifically, through electrophysiological measurements using planar lipid membranes, we characterize the kinetics of binding, as well its dependence on transmembrane voltage and the concentration of the blocker. In addition, we report a crystal structure of the KcsA–TBA complex, which helps to resolve some of the open questions posed by previous structural studies,[7,8] and reveals novel insights into the association of channel and blocker. Finally, we carry out an extensive conformational exploration of TBA bound inside the cavity of a reduced model of the KcsA channel using the Hamiltonian replica-exchange molecular dynamics method, in order to clarify the interpretation of the experimental observations. More generally, this study demonstrates the usefulness of a multidisciplinary approach in the study of complex processes in molecular biology.

Results

Electrophysiology measurements

The use of single-channel recordings generally permits dissection of an inhibitor action in mechanistic detail. However, under typical experimental conditions, the KcsA channel is biased strongly towards the closed state, and the resulting narrow dynamic range places severe restrictions on single-channel studies of blockers. The low probability of the channel being open results partially from inactivation; after being triggered to open from a resting, closed state, the channel enters an inactivated state from which it reopens only infrequently.[23,32] The probability of the channel being open is further decreased by the brief duration of the openings.[33,34] Previous work has shown that the dynamic range can be extended using two experimental manipulations; namely, threonine substitution of A108, and the use of Rb^+ as the permeant ion. The A108T mutation increases the open probability selectively by destabilizing a prominent closed state, without affecting the rate of ion conduction.[35] By contrast, Rb^+ dramatically stabilizes the conducting state of KcsA.[36] Although the underlying microscopic mechanism for the enhanced stability is unknown, Rb^+ is believed to traverse the selectivity filter using the same fundamental translocation steps as those used by K^+,[37] and it seems likely that the effect of Rb^+ on open time is a consequence of slight energetic differences in the way these two ions interact with the protein. Permeant ions are known to affect gating in a broad variety of channels;[38,39] for example, in eukaryotic channels, a "foot-in-the-door" mechanism has been proposed to explain the observation that Rb^+ prevents the channel from closing.[38]

As illustrated in Figure 1(a) and (b), bursts of A108T KcsA activity are interrupted by long non-conducting states, but within each burst the channel displays a high probability of being open. We focused our work on the effect of TBA on channel activity during the bursting behavior. Analysis of the dwell-time distributions within bursts reveals one open state and two closed states (Figure 1(c)). The single open state has an average lifetime of 55.9(±13) ms. The two closed states have average dwell times of 24.3(±3.5) ms and 0.5(±0.3) ms, and the longer closed state occurs at a slightly higher frequency (65.7(±19.1) %).

The recordings shown in Figure 2(a) illustrate the typical single-channel behavior in the absence and in the presence of TBA. Upon addition of TBA, a new non-conducting state dominates the closed dwell-time distributions. TBA acts as a slow blocker, with a $\tau_{blocked}$ of 9.0(±0.2) ms. In addition, the dwell time of the open state changes in a concentration-dependent manner (Figure 2(b)). Figure 3(a) shows the results from a closer examination of the concentration-dependence of on and off-rates at 200 mV. According to these data, the on-rate is concentration-dependent, while the off-rate is independent of concentration; namely, $8.8(\pm0.1)\times10^9$ M^{-1} s^{-1} and 93(±7) s^{-1}, respectively. The resulting disassociation constant, $K_d = k_{off}/k_{on}$, is therefore 10 nM; the apparent affinity of the KcsA–TBA complex is thus substantially greater than those measured in any of the eukaryotic K^+ channels.

Additional recordings made at 175 mV and 250 mV reveal another interesting feature of the TBA intracellular block. While the on-rate appears to

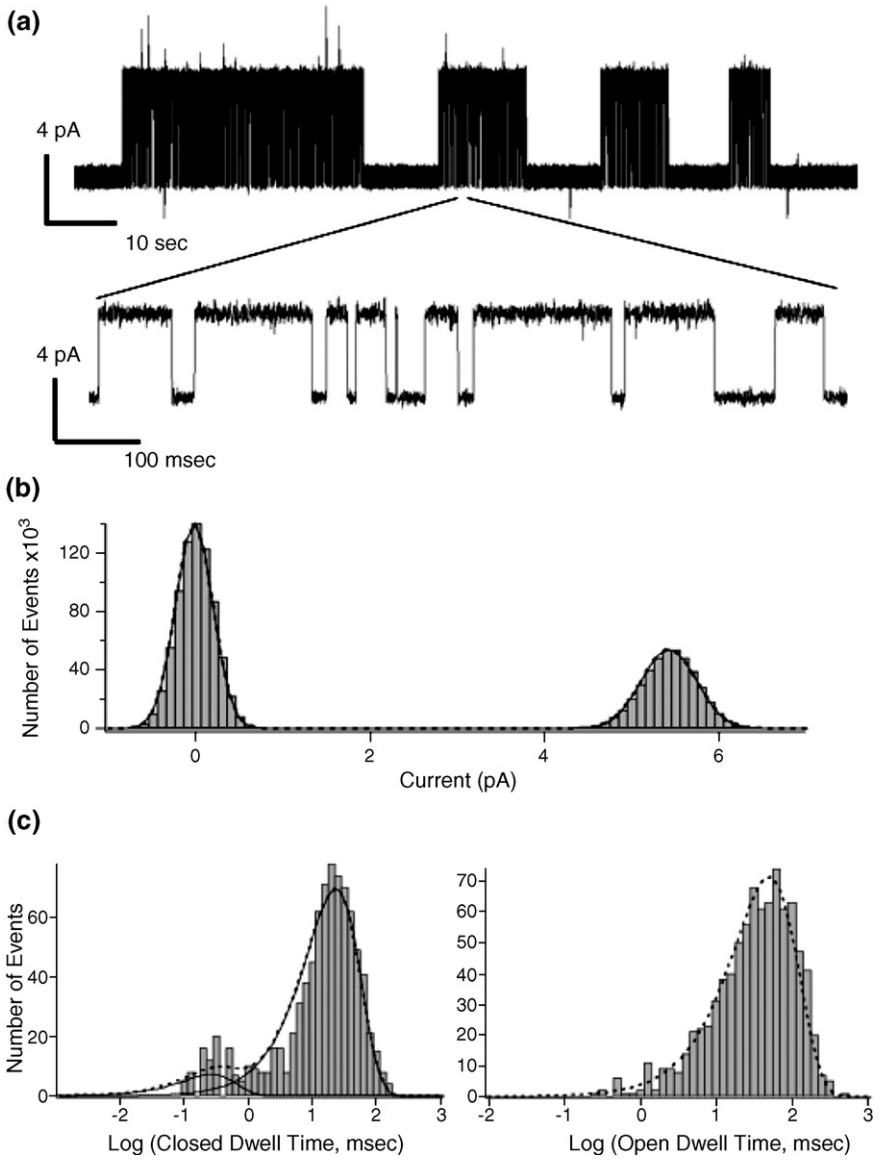

Figure 1. Properties of single-channel recordings from A108T-KcsA with 100 mM RbCl on both sides of the membrane. The pH of the intra- and extracellular solutions is 4.0 and 7.0, respectively. (a) The bursts of activity are interrupted by long non-conducting periods (top trace). The lower trace shows the activity during a burst in greater time-resolution. (b) All-point histogram of the open probability of the A108T channel, excluding the long-lasting, non-conducting state. The continuous line represents a Gaussian fit with two components. (c) Dwell-time histograms for the closed (left) and open (right) states. The closed dwell-time distribution was fitted with two exponentials (continuous lines), and the open dwell-time distribution was fitted with one; the overall fit is shown with broken lines.

be independent of voltage, the off-rate is voltage-dependent, increasing as the cytoplasmic face becomes more positive (Figure 3(b)). This result may seem somewhat counter-intuitive for a positively charged blocker accessing the channel from the intracellular side, since traditionally voltage-dependence is considered to arise from the driving force exerted by the transmembrane electric field on the blocker itself. As discussed below, previous theoretical analyses indicate that this assumption may not be justified in the current case,[40] and that the voltage-dependence may reflect indirect effects mediated by the permeant ions and/or the gating of the channel.[41]

X-ray crystallography

Crystals of the KcsA–Fab complex were grown in 150 mM KCl under saturating concentrations of TBA as described.[7] After data collection, processing and refinement, our 534 amino acid residue model of KcsA is very similar to the ligand-free structure reported by MacKinnon and co-workers (Figure 4(a)).[22] The RMS displacement of the C^α trace of the TBA-bound structure with respect to KcsA without TBA is 0.3 Å, which demonstrates that binding of TBA has little influence on the overall structure of the channel, as noted previously.[7] In addition, it was possible to locate four binding sites for K^+ in the

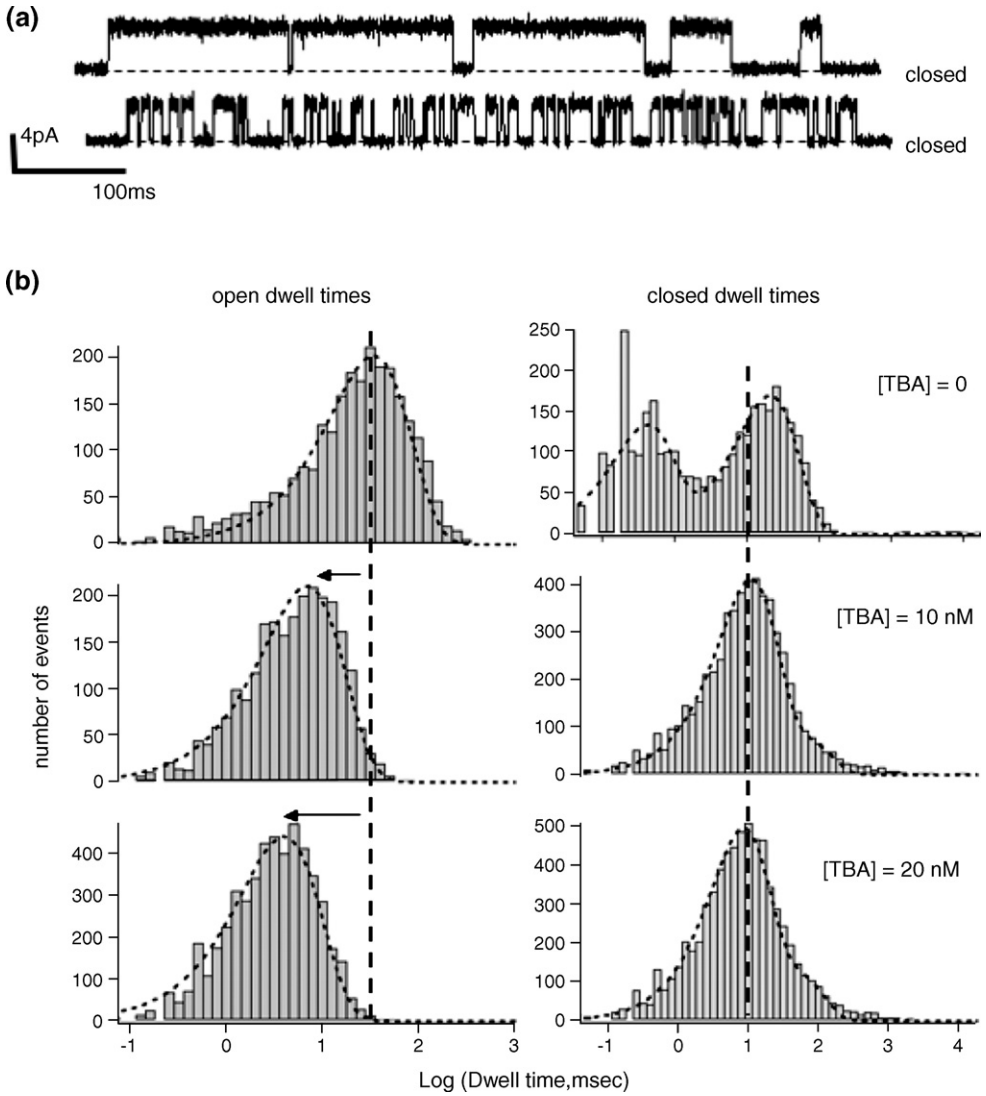

Figure 2. Effect of TBA on Rb^+ single-channel currents through A108T KcsA. (a) Single-channel current recording in the absence (top trace) and in the presence (bottom trace) of 20 nM TBA. (b) From top to bottom, dwell-time histograms of current recordings without TBA, with 10 nM TBA and with 20 nM TBA. The open dwell-times (left panels) decrease as the concentration of the blocker increases; note the displacement in the distributions (arrow) from the control value (vertical broken line). All three distributions are fitted with one exponential function. By contrast, a new component is observed in the closed dwell-time histograms (right panels) upon addition of TBA. A single-exponential fit is used for the closed dwell-time histogram in the absence of TBA; those in the presence of TBA require an additional exponential function.

selectivity filter, identical with those identified previously in the absence of TBA (Figure 4(b)).

The electron density shown in Figure 4 was calculated by molecular replacement, using the structure of KcsA (1K4C) with no TBA (it is an omit density map for the bound ligand). A well-resolved electron density attributed to TBA resembles a 4-fold cross lying parallel with the plane of the membrane within the central cavity of KcsA (Figure 4(c)). The cross is centered on the 4-fold symmetry axis of the channel, about 2 Å above what would be a binding site for K^+ in the absence of TBA.[21] The arms of the cross project away from the channel axis into the grooves created by I100 and F103. These residues form a ring of aromatic and hydrophobic contacts that appears to provide favorable van der Waals interactions, and that is analogous to the so-called φ-clamp facing the pore of the anthrax toxin, to which TBA also binds.[42] Residues corresponding to I100 and F103 have been shown to be crucial for the recognition of blockers or inactivation peptides by other K^+ channels.[7] In addition, the side-chain of T75 appears to provide stabilizing electrostatic interactions; residues corresponding to T75 in HERG and IKCa1 K-channel are implicated in modulating the binding of drugs like MK-499,[6] and TRAM-34,[2] respectively.

In the gas phase, TBA exists primarily in two stable conformations; namely, D_{2d}, with all four chains extended in a planar arrangement, and S_4, which is a tetrahedral structure.[43] The cross-shaped density observed in the crystal structure would thus appear to correspond to the D_{2d} conformation of TBA. Nevertheless, the electron density map derived from

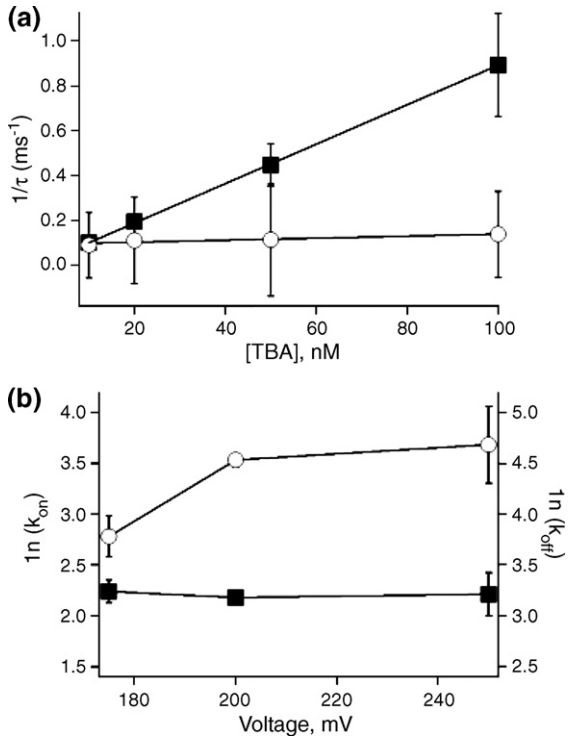

Figure 3. (a) Concentration dependence of TBA block. The on-rates are shown as filled squares and the off- by open circles. Both the on-rates and off-rates were fitted with a linear regression. Error bars represent the SEM. The data were generated from 4–11 datum points. (b) Voltage dependence of the TBA block. On-rate (filled squares) and off-rate (open circles) at 175 mV, 200 mV and 250 mV are shown. The data were generated from 4–11 datum points as in (a). The corresponding $z\delta$ is −0.3. Error bars represent the error of the linear regression used in the calculation of the rates.

our diffraction data also reveals a clear intensity peak at 5–6 Å below the centre of the cavity, in the vicinity of T107, where the pore becomes constricted (Figure 4(d)). A number of factors must be taken into consideration in trying to interpret the features of the electron density map. Firstly, TBA itself is not 4-fold symmetric in either the D_{2d} or S_4 forms. However, the symmetry of the crystal (space group *I*4, with the axis of symmetry along the axis of the channel) necessarily imposes an apparent 4-fold symmetry on the electron density of any bound ligand. Secondly, it is likely that the electron density results from a superposition of diverse configurations of TBA, provided that at least one of its alkyl chains lies on the plane of the membrane, while another projects down along the channel axis toward the bottom of the cavity. For example, it is possible that TBA adopts the S_4 conformation, oriented in the cavity as an inverted tetrahedron; alternatively, one or more orientations of the D_{2d} form of the molecule may be plausible.

A quantitative analysis of the dependence of the R_{free} values with the conformation of the ligand would, in principle, help to resolve this question. However, given the moderate resolution of the data set and the fact that TBA amounts to less than 0.5% of the atoms in the complex, it is very unlikely that a global indicator such as R_{free} would be sufficiently sensitive to multiple conformations of the ligand with any statistical significance. Moreover, this procedure is further complicated in the present case by the fact that the symmetry of the ligand and the channel are not alike, and that TBA is flexible and may depart from the ideal geometry in the bound form. Thus, it is not clear, on the basis of the crystallographic data alone, whether a unique or multiple binding modes exist.

Hamiltonian replica-exchange simulations

As mentioned above, QA compounds are known to adopt two main conformations in equilibrium, referred to as D_{2d} and S_4 (Figure 5(a)). Quantum-mechanical calculations have shown that, in terms of the intra-molecular potential energy, the D_{2d} form is preferred over S_4 by around 1 kcal/mol.[9,43] However, the greater degeneracy and conformational entropy of S_4 contribute importantly to the free-energy difference between these states, and at room temperature the gas-phase population ratio is predicted to be only marginally in favor of D_{2d} ($\Delta G \sim -0.2$ kcal/mol).[44] Nevertheless, in bulk water, the conformational equilibrium shifts strongly towards the D_{2d} state, due to its more favorable interactions with the solvent ($\Delta G \sim -1.5$ kcal/mol).[44]

On the basis of these observations, it is likely that the D_{2d} form will also be preferred in the solvated cavity of KcsA. However, interactions with the protein and the potassium ions in the selectivity filter may have a marked effect on the conformational equilibrium of the blocker. To determine the extent to which the S_4 form is present in the equilibrium, we carried out two independent simulations (SIM#1 and SIM#2), where the starting configuration of TBA within the KcsA model was either D_{2d} or S_4, and analyzed the evolution of each population. Given the large energy barriers between the two forms of TBA (Figure 5(a)), and the close confinement of the water-filled cavity (Figure 5(b)), it was necessary to implement an advanced sampling technique, known as Hamiltonian replica-exchange, to enable the molecule to undergo reversible transitions between both states (see Materials and Methods for further details). The simulation time of both SIM#1 and SIM#2 was 40 ns per replica, and 23 replicas were used in each.

The outcome of these simulations is summarized in Figure 5(c), where we analyze the time-evolution of the conformational equilibrium of TBA in terms of an order parameter η that discriminates between the D_{2d} and S_4 states.[44] As can be seen, the population of S_4 in the simulation where TBA starts in the S_4 conformation (SIM#1) decreases gradually until the D_{2d} form is the most prominent in the equilibrium. (Note that at the beginning of this simulation all replicas in the Hamiltonian replica-exchange molecular dynamics (HREMD) simulations simulation ensemble are in S_4, and thus no D_{2d} is present.)

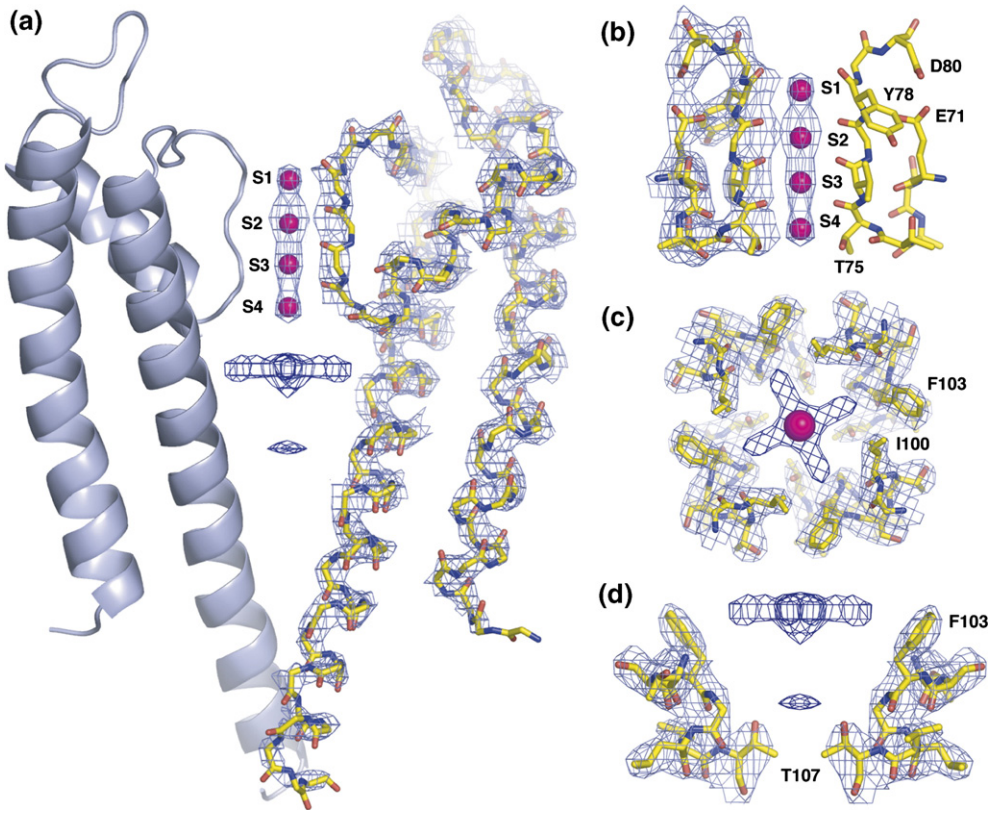

Figure 4. Crystal structure of wild-type KcsA in complex with TBA and potassium. (a) The backbone of two of the four protein monomers, viewed from the plane of the membrane, alongside the binding sites for K^+ (magenta) and the electron density corresponding to TBA. The σ-weighted $2F_o–F_c$ maps are contoured at 2.5σ (protein), 3.5σ (ions) and 0.5σ (blocker), and drawn as a blue mesh. (b) A close-up view of the selectivity filter and the potassium-binding sites; the $2F_o–F_c$ maps are contoured at 1.5σ (protein) and 3.5σ (ions). (c) and (d) Electron density corresponding to TBA (contoured at 0.5σ), viewed down the 4-fold symmetry axis of the channel, or from the plane of the membrane. The molecular graphics in Figures 4–7 were rendered with Pymol [http://pymol.sourceforge.net/].

Consistently, the simulation in which TBA starts in the D_{2d} conformation (SIM#2) remains in this state; only some of the replicas with a modified Hamiltonian undergo rare transitions to the S_4 state (not shown).

Having established that, according to our model, TBA is primarily in the D_{2d} form while in the water-filled cavity of KcsA, we proceeded to investigate in more detail whether multiple binding modes exist, as well as whether these may be energetically coupled to the potassium ions in the selectivity filter. To this end, we carried out two additional HREMD simulations where a potassium ion was located either in site S3 or in site S4 within the selectivity filter (SIM#3 and SIM#4, respectively). In both simulations, the initial conformation of TBA across the replica ensemble was that in the D_{2d} state, oriented at random within the cavity (but not in the plane of the membrane).

Simulations SIM#3 and SIM#4 included 23 replicas, and were extended up to 100 ns per replica in order to gather enough sampling data to construct a density map that could be compared to the crystallographic data. To compute this density map, we simply mapped each of the configurations of TBA onto a three-dimensional grid comprising the binding cavity, using a mass-weighted, tri-linear scheme; from these data, we subsequently derived iso-density contours. As a qualitative measure of the convergence of the sampling, we monitored the degree to which the computed density maps adopted the 4-fold symmetry of the channel.

The resulting mass density maps are shown in Figure 6, contoured at 20% of the maximal density computed. When the nearest K^+ in the selectivity filter resides in S3, the computed density resembles the experimental cross-shaped electron density observed at the top of the cavity (Figures 4(c) and (d), and 6(a) and (b)). Underlying this ensemble-averaged density there are a diverse range of configurations of TBA (though the D_{2d} form is preserved throughout both SIM#3 and SIM#4), the most likely of which are those where TBA does indeed lie in the plane of the membrane and is centered on the axis of the channel (Figure 6(c) and (d)). Nonetheless, other orientations where one or more of the alkyl chains of TBA is not in the plane of the membrane (Figure 7) also contribute to the computed density, by virtue of the 4-fold symmetrizing effect of the averaging.

The ensemble-averaging effect that underlies both the computation and the X-ray diffraction experiment is illustrated even more clearly when the nearest K^+ is located in site S4 of the selectivity filter.

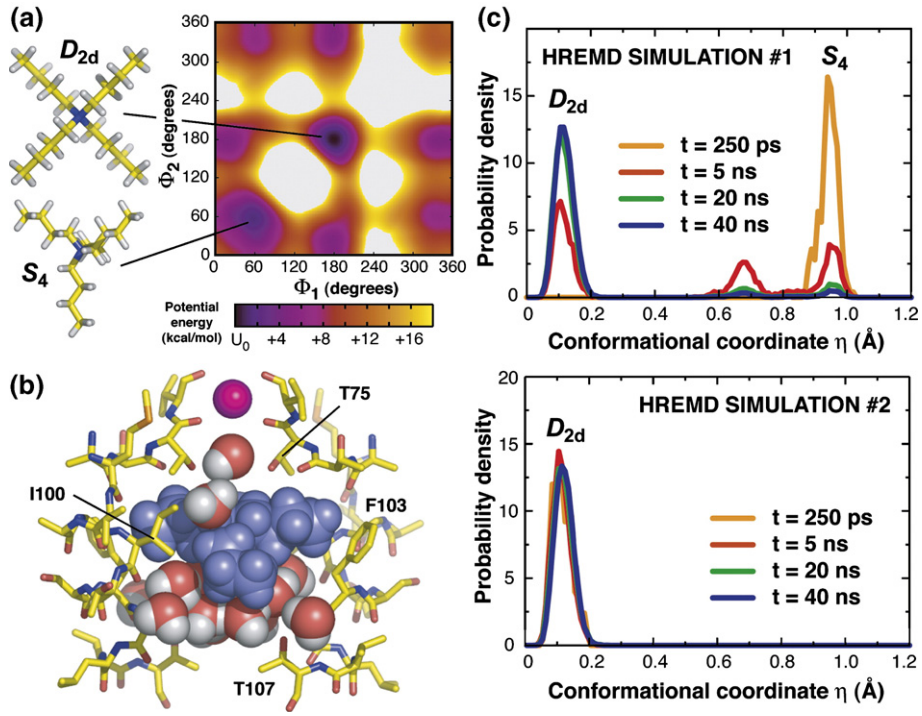

Figure 5. (a) D_{2d} and S_4 conformations of TBA, alongside a projection of the potential-energy surface along two of the C^{α}-N-C^{α}-C^{β} dihedrals whose rotation describes the transition between these states. (b) Reduced model of the KcsA channel used in the Hamiltonian replica-exchange simulations; the system includes a potassium ion in the selectivity filter (magenta sphere), in site S3 or S4, a TBA molecule (blue spheres) and 15 water molecules. (c) Time-dependence of the populations of the D_{2d} and S_4 states of TBA in two independent replica-exchange simulations. In simulation SIM#1, all replicas start out in the S_4 conformation, but gradually the D_{2d} state becomes predominant in the equilibrium. In simulation SIM#2, all replicas start out in the D_{2d} state and no transition to the S_4 state is observed.

In this case, TBA is rarely in the plane of the membrane (Figure 6(h)); rather, most configurations feature a pronounced tilt, and TBA is centered off-axis, and a few ångström units lower than in the previous case (Figure 6(g)). Nonetheless, the resulting ensemble average still features the four arms in a symmetric arrangement (Figure 6(f)) and, as a result of the tilted orientation, a fifth arm in the computed density projects down the axis of the channel, with maximal intensity close to the endpoint (Figure 6(e)). A series of representative configurations from SIM#3 and SIM#4 are depicted in Figure 7.

Since in reality the protein crystal contains channels in which the potassium ions detected in the selectivity filter are in sites S1 through S4, the measured electron density most likely reflects the superposition of two states of the KcsA–TBA complex, each corresponding to the S1/S3 or S2/S4 ion configurations. Indeed, combination of the computed density maps derived from SIM#3 and SIM#4 in a 5:2 ratio (see Discussion) results in the density map drawn in Figure 8(a) and (b), which is in very good agreement with the crystallographic data, considering the simplicity of the model and the possible effects of the fast freezing of the crystals. As in the experiment, the simulation yields the cross-shaped density volume at the top of the cavity, somewhat extended downwards along the channel axis, as well as a small peak of density in the vicinity of T107. In Figure 8(c)–(f), two representative configurations of TBA from the simulated ensemble are overlaid on the experimental density maps; note that in both cases TBA is in the D_{2d}, planar-like state, and yet, the possibility of a tilted orientation within the cavity of the channel, combined with the symmetrizing effect of the lattice averaging, gives rise to a measured density map that in fact originates from at least two distinct binding modes of TBA.

Concluding Discussion

Tetrabutylammonium is known to block eukaryotic K^+ channels with varying affinities. This variation is mainly due to the wide range of on-rates observed (10^3–10^7 M^{-1} sec^{-1}). The off-rates, on the other hand, are relatively similar, at around 10–200 s^{-1}.[45–48] The comparatively high on-rate observed here for KcsA (ca 10^{10} M^{-1} s^{-1}) results in an apparent affinity that is greater than that measured previously for any of the eukaryotic K^+ channels. In theory, this could result from our use of Rb^+ as a permeant ion. However, given the homology of the pore-lining residues among this family of proteins, we propose that the greater affinity arises not so much from stronger interactions between the blocker and the channel, but rather from the greater accessibility of the binding cavity in the case of KcsA. This notion is consistent with the fact that KcsA lacks the large intracellular domains that are linked to the trans-

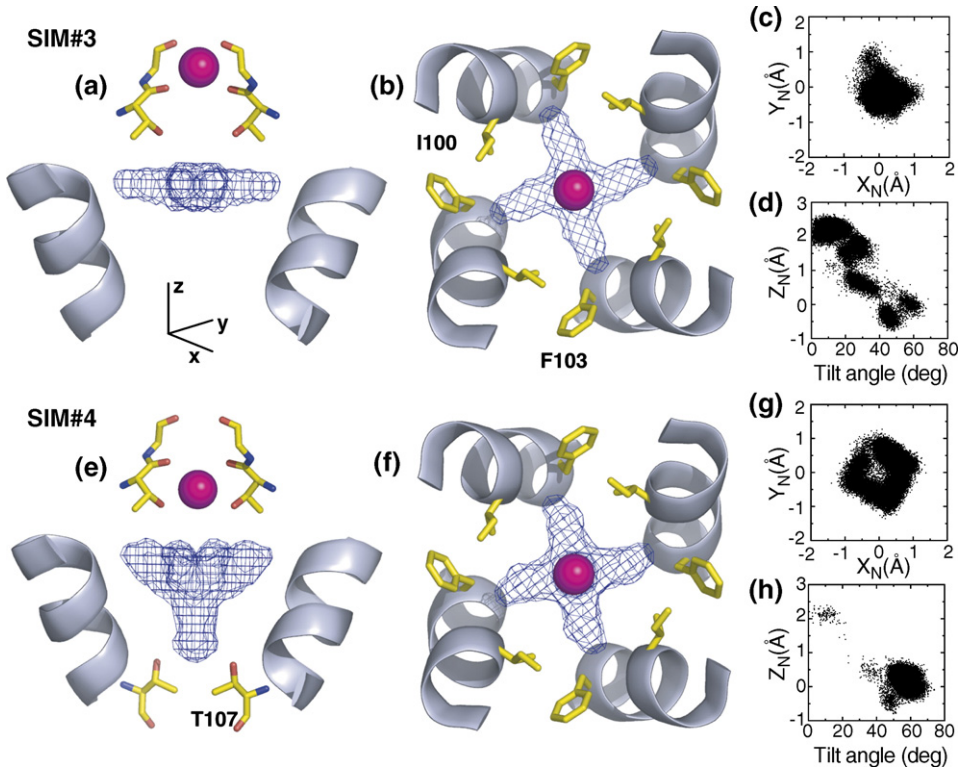

Figure 6. (a) and (b) Density maps derived from the ensemble of TBA configurations obtained in simulation SIM#3, where a potassium ion is located at site S3 in the selectivity filter. (c) Projection on the membrane plane of the coordinates of the nitrogen atom of TBA in all configurations in the simulated ensemble. (d) Correlation of the *Z*-coordinate of the nitrogen atom of TBA and the tilt of the molecule relative to the plane of the membrane, for all configurations in the simulation ensemble. The plane of TBA is defined by a least-squares fit relative to coordinates of the N and C^{β} atoms. (e)–(h) Same as above, but for simulation SIM#4, where a potassium ion is located in site S4 in the selectivity filter.

membrane segment in other K^+ channels, which presumably constitute a kinetic barrier for the translocation of the blocker from the bulk to the entrance of the pore. The subsequent binding event, which results in the actual blockage of the ionic current, is probably energetically comparable across the family of K^+ channels, as reflected by the similarity of the off-rates.

An intriguing aspect of the blocking properties of TBA is the voltage dependence of the binding kinetics, which at first sight appears to be counter-intuitive, in that more positive voltages (in the intracellular side) lead to faster off-rates. However, this result can be rationalized, bearing in mind that, in the context of the lipid membrane, transfer of TBA to and from the external solution can take place only while the channel is in the open state, even though, as shown by the crystal structure, the channel can close in the presence of the blocker. In this open state, the drop in the transmembrane voltage is

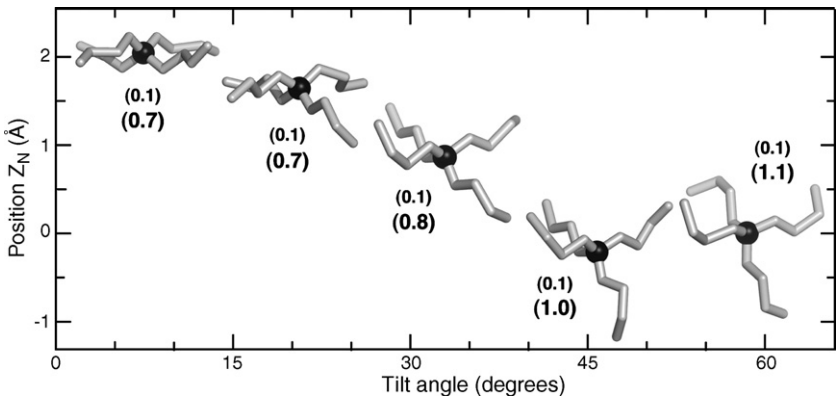

Figure 7. Representative configurations of TBA within the transmembrane cavity of KcsA, extracted from simulations SIM#3 and SIM#4. The configurations are ordered according to the tilt of the molecule relative to the plane of the membrane and to the position of the nitrogen atom of TBA along the axis of the channel ($Z=0$ corresponds approximately to the location of the binding site for K^+ in the absence of TBA). For each tilt, the characteristic RMS deviation (in Å) with respect to the ideal, all-*trans* D_{2d} geometry (Figure 5(a)) is provided, derived from an ensemble average. The number at the top corresponds to the C_8N^+ core (which defines the conformational state, i.e. D_{2d} *versus* S_4); the number at the bottom corresponds to all non-hydrogen atoms in the molecule.

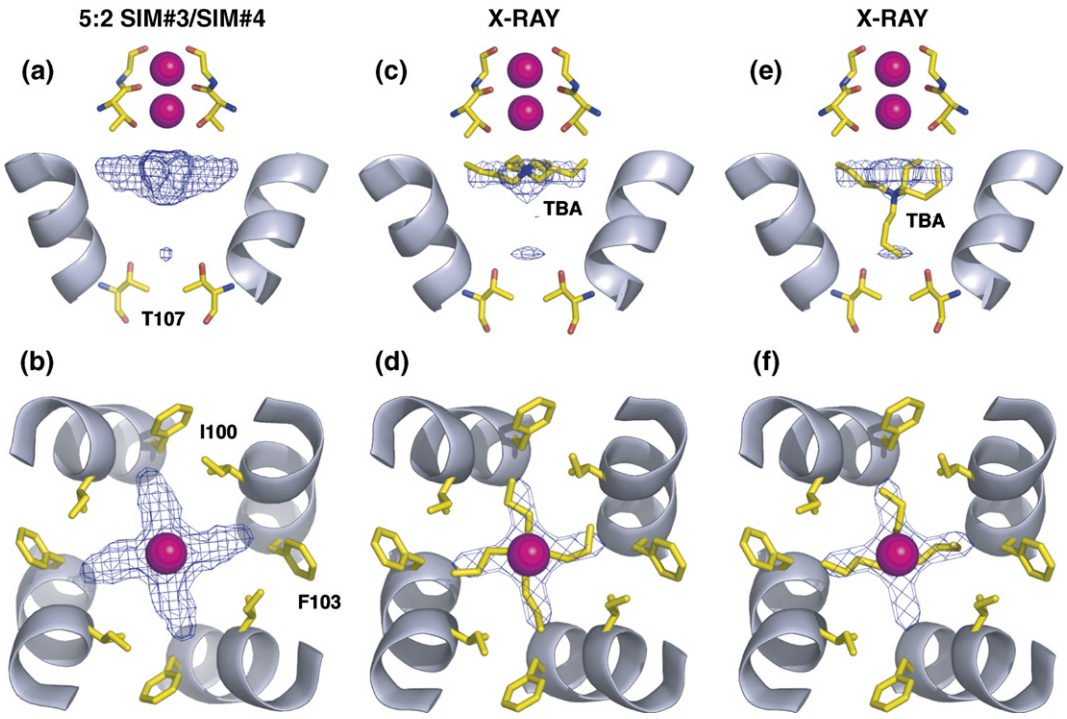

Figure 8. (a) and (b) Density maps derived from the ensemble of TBA configurations obtained in simulations SIM#3 and SIM#4, combined in a 5:2 ratio. (c) and (d) Experimental electron density map for TBA (contoured at 0.5σ), alongside a configuration of TBA chosen randomly from those of tilt smaller than 10°, relative to the plane of the membrane. (e) and (f) Experimental electron density map for TBA (contoured at 0.5σ), alongside a configuration of TBA chosen randomly from those of tilt equal to around 60°. Note that in both cases TBA is in the D_{2d} state, which is preserved throughout simulations SIM#3 and SIM#4.

concentrated in the selectivity filter region,[40] and thus the magnitude of the electric field in the binding cavity is minimal. This is consistent with the observations that the on-rates are voltage-independent; i.e. the transmembrane voltage does not drive the blocker into the cavity. Thus, the voltage-dependence of the off-rates must arise indirectly from the effect that voltage may have on the kinetics of channel gating.

It has been shown that the voltage-dependence of the block can be altered radically by interaction between the blocker and the permeant ions.[31,41] In this work, we show through computer simulations and X-ray crystallography that TBA binds in two modes, and that the relative populations of these modes appear to be coupled to the configuration of the potassium ions in the selectivity filter. In particular, a tilted arrangement of TBA relative to the plane of the membrane is more favored when the nearest potassium ion resides in site S4, whereas an orientation along the plane of the membrane is more favored if the nearest potassium ion is located in site S3. This trend is thus consistent with the electrostatic repulsion between the blocker and the permeant ions. In the latter arrangement, TBA interacts solely with residues at the top of the cavity (T75, I100, and F103); by contrast, in the tilted orientation, it also contacts the hydrophobic group of T107, which constricts the pore when the channel is closed.

On the basis of these observations, we hypothesize that the observed dependence of the off-rate on the transmembrane potential arises from the influence of the electric field on the ion configuration in the selectivity filter, which in turn affects the extent to which TBA may interfere with the gating of the channel through its interaction with T107. That is to say, the smaller the transmembrane potential, the greater the probability of having a K^+ in site S4, which, in turn, would increase the probability that TBA adopts a tilted orientation. In this orientation, the hydrophobic interaction of TBA and T107 may hinder the stochastic opening of the channel, thus slowing the off-rates. More positive voltages would have the opposite effect on the off-rates, by indirectly promoting a binding mode where TBA lies on the plane of the membrane, and therefore does not interfere with the gating kinetics.

Another important conclusion of this work pertains to the extent to which TBA binding affects the structure of the channel, which has been an open question until now. The structure of KcsA with bound TBA at 2.9 Å resolution was solved by MacKinnon and co-workers.[7] In this crystal structure, KcsA is unchanged with respect to the ligand-free, closed-state form, and TBA can be identified clearly within the transmembrane cavity. However, the electron density corresponding to TBA is featureless, which precludes the elucidation of the conformation of the molecule, its orientation within the cavity, or its interactions with pore-lining residues in the channel. Subsequent crystallographic studies of a KcsA–Fab antibody complex in the

presence of Tl^+ by Gross and co-workers succeeded in resolving TBA in molecular detail; namely, in a configuration where the molecule lies on the plane of the membrane.[8] Nevertheless, their structure reveals substantial changes in the conformation and ion occupancy of the selectivity filter, as well as at the top of the binding cavity.

In this work, the use of K^+ as the permeant species as well of the Fab antibody fragment to aid the crystallization has enabled us to resolve TBA in molecular detail, as well as to assess the structural impact that the blocker may have, under more physiological conditions. On the basis of the resulting crystal structure, we concur with Zhou *et al.*, in that the TBA blocker does not alter the structure of the channel *per se* when the selectivity filter is occupied by potassium ions. Therefore, the structural changes observed by Lenaeus *et al.*[8] must then be attributed to the presence of Tl^+, or to the combined effect of TBA and Tl^+. In addition, the structure reported by Gross and co-workers did not reveal the additional peak of density in the vicinity of T107 that is observed clearly in our data. It is plausible that the single occupancy of the selectivity filter in their case enhances the likelihood of a single orientation near the top of the cavity.

In a broader sense, the present study illustrates the usefulness of computer simulations as a complementary tool in biological chemistry. To tackle the intrinsic difficulties associated with the conformational free-energy barriers of TBA and the close-confinement of the water-filled cavity of KcsA, we have used an advanced but computationally costly simulation method, which in turn requires a simplification of the model system. Simulations with more sophisticated models incorporating long-range electrostatic effects, or alternative force field parameters for TBA such as those described by Luzhkov *et al.*[43] could alter the relative stability of the S_4 and D_{2d} forms and the coupling between the TBA and the ions occupying the selectivity filter, though the main results from the present work are expected to remain valid. In practice, different treatments would simply affect the 5:2 ratio assigned to the computed density maps in Figure 6(a) and (b) (leading to that in Figure 8(a)), but the shape of the simulated maps of bound TBA would remain qualitatively unchanged. Seeking quantitative agreement with the relative populations of the configurations of the protein-ion-blocker system in the complex environment of crystals that are fast-frozen in liquid nitrogen is not the purpose of the present analysis. The fact that good agreement is found between the crystallographic and computed density maps with a single adjustable parameter is strong support for the present interpretation of the data; namely, (a) TBA can bind into the cavity of KcsA by adopting multiple conformations, dominated by the D_{2d} conformer in an in-plane and a tilted orientations, and (b) the relative population of these binding modes is sensitive to the configuration of the ions occupying the selectivity filter.

Materials and Methods

Electrophysiology measurements

Materials

All salts used were reagent grade or higher. Unless stated otherwise, high-purity chemicals were purchased from Sigma-Aldrich (St. Louis, MO). Mops was obtained from American Bioanalytical (Natick, MA), TBA was from Fluka (Milwaukee, WI), Rb_2Succinate was from Great Western Inorganics (Arvada, CO). *n*-Dodecyl-β-D-maltoside (sol-grade) was used for protein extraction and purification; lipid for reconstitution was solubilized with Chaps (anagrade) from Anatrace (Maumee, OH). Lipids for the reconstitution into vesicles and for planar lipid bilayer experiments were 1-palmitoyl-2-oleoyl-sn-glycero-3-phosphoethanolamine (POPE) and 1-palmitoyl-2-oleoyl-sn-glycero-3 [phospho-rac-(1-glycerol)] (sodium salt) (POPG) from Avanti Polar Lipids (Alabaster, AL). *Escherichia coli* strain JM-83 was purchased from ATCC (Manassas, VA). The cells were grown in Terrific broth (TB: per liter; 12 g of Tryptone, 24 g of yeast extract, and 4 ml of glycerol, with 17 mM KH_2PO_4 and 72 mM K_2HPO_4). Solutions for bilayer experiments were prepared daily in the following two ways: (1) 96 mM RbCl and 10 mM succinic acid (*trans* solution) or 10 mM Mops (*cis* solution); the pH was adjusted to 4.0 (*trans* solution) or 7.0 (*cis* solution); (2) For the *trans* solutions, we used 10 mM Rb_2Succinate and 80 mM RbCl; the pH was adjusted to 4.0 using HCl.

Expression, purification and reconstitution of KcsA

For the plasmid construct for expression of KcsA, we used a synthetic gene encoding the native protein sequence with an additional N-terminal His_6 tag. This gene was inserted into the pASK90 expression plasmid (generously supplied by Dr Arne Skerra); expression was induced by the addition of anhydrotetracycline (aTC; Acros Organics, Morris Plains, NJ). Wild-type and mutant KcsA proteins were expressed and purified as described.[31] After induction, cells were incubated for 2 h to allow for the expression of the protein. Cells were then washed and resuspended in buffer A (95 mM NaCl, 5 mM KCl, and 50 mM Mops, adjusted to pH 7.0 with NaOH), protease inhibitors were added (final concentrations were 1 μM leupeptin, 1 μM pepstatin A, 0.5 mM PMSF), and cells were disrupted by a French press. Unbroken cells were cleared by centrifugation at 12,000*g* for 25 min, and membranes were isolated by ultracentrifugation at 75,000*g* for 45 min. Membranes were resuspended in buffer B (95 mM NaOH and 5 mM KCl, adjusted to pH 7.0 with H_3PO_4) and extracted using 15 mM dodecyl maltoside for 30 min. The unsolubilized membranes were removed by ultracentrifugation at 75,000*g* for 45 min. The protein was purified using Ni affinity chromatography (Ni-NTA Agarose, Qiagen); the extracted membranes were incubated with the agarose beads for 2 h in the presence of 40 mM imidazole, washed with 40 mM imidazole and eluted with 400 mM imidazole. For reconstitution, lipid (7.5 mg/ml of POPE and 2.5 mg/ml of POPG) was solubilized after incubation with 34 mM Chaps for 2 h at room temperature. From 1-4 μg of protein was mixed immediately after purification with 400 μl of solubilized lipid and incubated at room temperature for 20 min. Detergent was removed using a

20 ml Sephadex G-50 column; fractions of 500 μl were collected and those containing the vesicles were determined by visual inspection and were stored at −80 °C for up to a month.

Single-channel recordings

Single-channel recordings were performed in a horizontal planar lipid bilayer setup. Partitions made from overhead transparency film having holes roughly 50 μm in diameter were treated by application of ~0.2 μl of lipid solution (15 mg/ml of POPE and 5.0 mg/ml of POPG in decane), followed by drying in air for 20 min. After the chambers were filled with solution, bilayers were formed by painting with a glass rod dipped in the lipid solution. The reconstituted protein was added to the *cis* chamber, and the bilayer was formed with the bubble expelled by the pipet after the addition of sample. The orientation of the recording system is such that the *cis* chamber, containing solutions at pH 7, is equivalent to the periplasmic surface of the protein, while the intracellular surface of the channel faces the *trans* chamber. Voltages and currents follow the standard electrophysiological convention, with extracellular solution at ground voltage.

Currents were sampled at 20 kHz or 50 kHz, low-pass filtered at 2 kHz and further filtered digitally at 1 kHz before data analysis (the effective filtering frequency corresponds to 0.9 kHz).[49] Data were acquired and analyzed with Clampex and P-stat software (Axon Instruments). Dwell time distributions were fitted with one or more exponential components using a least-squares fitting procedure.

Single channel records of the KcsA channel display bursts of activity that are interrupted by long closed/inactive states (ca 10–15 s). During a given burst, the channel alternates between open and closed states that have much shorter lifetimes than the typical duration of the bursts and of the long closed/inactive states. The following analysis of the block experiments by TBA corresponds to the time-period within bursts. Let us denote the closing and opening rates of the channel in the absence of TBA as $k_{open}=1/\tau_{close}$ and $k_{close}=1/\tau$, where τ_{open} and τ_{close} are the open and closed dwell times, respectively. In the presence of a slow blocker, the exit rate from the open state will be the sum of the rates of closing of the channel and the on-rate of blocker. Therefore, the on-rate of the blocker can be calculated as:

$$k_{on} = \left(\frac{1}{\tau^{B}_{open}} - \frac{1}{\tau_{open}}\right)\frac{1}{[TBA]}$$

where τ^{B}_{open} is the open dwell time in the presence of the blocker. The off-rate is expected to be concentration-independent and equal to $1/\tau_{blocked}$, where $\tau_{blocked}$ is the dwell time of the blocked state (which may differ significantly from τ_{close} in the absence of the blocker). Finally, the dependence of the block with the applied transmembrane voltage is given by:

$$\ln k(V) = \ln k(0) - \frac{z\delta FV}{RT}$$

where k denotes either the on-rate or the off-rate, z is the unitary charge moving in the electrical field, δ is the fraction of voltage across which the charge moves, R is the gas constant and T is absolute temperature.[50]

Crystallography and X-ray diffraction

Purification of wild-type KcsA and Fab antibody fragment

KcsA was expressed and purified as described,[22] and eluted with 500 mM imidazole. To remove excess imidazole, overnight dialysis was carried out in 50 mM Tris–HCl (pH 7.5), 150 mM KCl, 10 mM dodecyl maltoside. The C-terminal flexible end with His_6 tag (35 amino acid residues) was excised from KcsA using chymotrypsin, by incubating KcsA and chymotrypsin at a ratio of 15:1 (w/w), respectively, for 2 h at room temperature. All chemicals were bought from Sigma-Aldrich, except detergent, which was purchased from Anatrace.

Hybridoma cells containing monoclonal antibodies raised against the extracellular epitope of KcsA were generously provided by Roderick Mackinnon. The Sloan-Kettering Monoclonal Antibody facility provided IgG in serum after harvesting the hybridoma cells that had been provided to them. An affinity column was used to separate IgG from serum protein A, using a phosphate buffer at pH 7.0 and eluted with a pH gradient from 7.0 to 3.0 (citrate buffer). The Fab fragment of the antibody was obtained through proteolysis, through incubation of the protein with papain at a 250:1 (w/w) ratio at 37°C for 3 h. The reaction was stopped by adding 50 mM iodoacetamide. Excess iodoacetamide was subsequently removed through overnight dialysis in 20 mM Tris–HCl pH (7.5). Fab and F_c fragments were separated on an ion-exchange chromatography column (Mono-Q), where Fab comes out in the flow through. Fractions were concentrated to 2–4 mg/ml and stored at −80 °C.

Formation of KcsA–Fab complex

After digestion by chymotrypsin, wild-type KcsA was incubated with purified Fab for 30 min. The complex was then injected into a size-exclusion chromatography column (AKTA FPLC with 200 HR Sepharose), which is equilibrated with 50 mM Tris–HCl (pH 7.5), 150 mM KCl, 5 mM dodecyl maltoside. The complex comes out as a single peak at ~12.2 ml. Fractions were pooled in and concentrated to 10–12 mg/ml using 30 kDa cutoff filters. Before setting up the trays for crystallization, purified KcsA-Fab complex (10–12 mg/ml) in 50 mM Tris–HCl (pH 7.5), 150 mM KCl, 5 mM dodecyl maltoside was incubated with 5 mM TBA (purchased from Sigma) at room temperature for 30–60 min.

X-ray crystallography

Crystals were obtained after two to three days in a sitting drop containing 20–25% (w/v) PEG 400, 50 mM magnesium acetate and 50 mM sodium acetate (pH 5.4–5.6) at 20 °C. In the same drop, cryoprotection was achieved by increasing the concentration of PEG 400 from 20–25% to 40%. After cryoprotection, crystals were frozen in liquid nitrogen and shot at the X4A beam line of the National Synchrotron Light Source, diffracting to a Bragg spacing of 2.9 Å. Data were processed with Denzo and Scalepack.[51] Phases were obtained by molecular replacement using the structure of the KcsA-Fab complex solved by Zhou *et al*.[22] CNS[52] was used to refine the model of the structure of TBA-bound KcsA (a TBA molecule was not explicitly included in the model during refinement), at 2.9 Å resolution and 81% completeness. (An alternative refinement at 3.3 Å and 90% completeness was carried out, which yielded an analogous omit density map for TBA.)

Further details on the data collection and refinement statistics are given in Table 1.

Molecular dynamics simulations of the KcsA-TBA complex

Description of the simulation system

The simulations of the KcsA–TBA complex used a reduced model of the protein comprising a 4-fold symmetric tetramer of residues 73–76 and 96–107 (PDB code 1K4C), alongside a single K^+ ion in the selectivity filter, located either in site S3 or site S4. The interior of the cavity was solvated with 15 water molecules, following two independent grand canonical Monte Carlo simulations of the KcsA–TBA complex analogous to those described by Woo *et al*.[53] where TBA is in either of its two main conformational states, D_{2d} or S_4. This number is consistent with the observation that under constant room pressure TBA displaces around 16 water molecules in bulk liquid (not shown), while the cavity of KcsA can hold approximately 30 water molecules.[53] All atoms in the channel as well as the potassium ions were fixed in space during the simulations, whereas both TBA and the water molecules were free to move. While this choice merely reflects the need to reduce the computational cost of the simulations to improve the convergence of the calculations, it is perfectly consistent with the fact that the structural changes induced by TBA on the channel are negligible, as is shown in this paper and elsewhere.[7] Independent simulations of the complex using flexible side-chains are also supportive of this approximation (not shown). Finally, analysis of long-range electrostatic effects from the environment using the generalized solvent boundary potential framework[54] indicates that the population of the in-plane binding orientation would be somewhat increased relative to the reduced model (not shown), though the qualitative trends remain unchanged.

Table 1. Data collection and refinement statistics of the crystal structure of the KcsA-TBA complex

A. *Data collection*	
Space group	*I*4
Cell dimensions	
a (Å)	156.20
c (Å)	75.316
Resolution (Å)	50.0–2.9
Completeness[a] (%)	80.8 (53.8)
B. *Refinement*	
Number of reflections	16,622
R_{work}[b] (%)	22.5
R^b_{free} (%)	28.4
Number of atoms	
Protein	4074
Ion	4
Ligand[c]	34 (two models)
Water	11
B-factors	
Protein (Å^2)	50.29
Ion (Å^2)	27.13
Water (Å^2)	42.16
RMSD from ideal	
Bond lengths (Å)	0.008
Bond angles (deg.)	1.377

[a] Values in parentheses are for the highest-resolution shell (3.1–2.9 Å).
[b] $R_{work} = \sum \mid F_o - F_c \mid / \sum F_o$, 10% of the data were excluded from the refinement and used in the calculation of R_{free}.
[c] Two models of the TBA molecule are fit into the observed density without any refinement.

Hamiltonian replica-exchange molecular dynamics (HREMD) simulations

To enhance the extent of the conformational sampling, the simulations of the KcsA–TBA complex were carried out under the Hamiltonian replica-exchange framework.[44,55,56] In the HREMD scheme, the simulation is coupled to an ensemble of additional simulations of the same molecular system, which are designed to access relevant regions of the configurational space more easily. In particular, these additional simulations, or replicas, have a different potential-energy function, each of which is chosen so as to gradually reduce the energy barriers characteristic of the system under study. By allowing the exchange of configurations between the replicas and the main simulation, the latter will have a much better chance of exploring all the important regions of the configurational space. Nonetheless, to ensure that the all simulations in the replica system remain in the appropriate thermodynamical ensemble in spite of their coupling, it is crucial to regulate the exchange of configurations through the following exchange probability p_{ex}:

$$p_{ex}(i,j) = \begin{cases} 1 & \text{if } \Delta(i,j) \le 0 \\ \exp(-\Delta(i,j)) & \text{if } \Delta(i,j) > 0 \end{cases}$$
$$\Delta(i,j) \equiv \beta_i[U_i(\mathbf{X}_j) - U_i(\mathbf{X}_i)] + \beta_j[U_j(\mathbf{X}_i) - U_j(\mathbf{X}_j)]$$

where the indices i and j denote a given pair of replicas, $\beta_\iota = 1/k_B T_i$, and U_i and $\mathbf{X}_i$ are the potential energy function and the spatial configuration of replica i. Further details of the derivation of p_{ex} and the implementation of the HREMD framework are given by e.g. Faraldo-Gómez & Roux.[44] In the current case, the potential-energy function across the replica ensemble was modified through a scaling factor λ; namely:

$$U = U_{TBA} + U_{PROT} + \lambda U_{WAT} + \lambda^3 U_{TBA-WAT} + \lambda U_{TBA-PROT} + \lambda U_{PROT-WAT}$$

where $U_{TBA} = U_{bonds} + \lambda U_{angles} + \lambda U_{torsions} + \lambda U_{elec} + \lambda U_{vdw}$. The number of replicas used in all HREMD simulations was 23, with λ between 1.00 and 0.10. The corresponding pair-wise exchange acceptance ratio ranged from 35% to 60%. All simulations were carried out with a modified version of the CHARMM C32A2 molecular simulation software,[57] using its Langevin-equation integrator with a collision frequency of 5 ps^{-1}, at $T = 300$ K. Parameters were adapted from the CHARMM22 force field,[58] as described.[9,44]

Protein Data Bank accession number

The crystal structure of KcsA, and two representative configurations of TBA extracted from the replica-exchange simulations, has been deposited in the RCSB Protein Data Bank, with accession number 2HJF.

Acknowledgements

We are grateful to the staff at the Brookhaven National Lab X-4A beamline for their assistance, and to R. Mackinnon (Rockefeller University) for

providing us with the KcsA monoclonal antibody hybridoma cell-line. Computational resources for this project were provided, in part, by the Institute for Computational Biomedicine of the Weill Medical College of Cornell University.

References

1. Armstrong, C. M. (1974). Ionic pores, gates, and gating currents. *Quart. Rev. Biophys.* **7**, 179–210.
2. Wulff, H., Miller, M. J., Hansel, W., Grissmer, S., Cahalan, M. D. & Chandy, K. G. (2000). Design of a potent and selective inhibitor of the intermediate-conductance Ca^{2+}-activated K^+ channel, IKCa1: a potential immunosuppressant. *Proc. Natl Acad. Sci. USA*, **97**, 8151–8156.
3. Spector, P. S., Curran, M. E., Keating, M. T. & Sanguinetti, M. C. (1996). Class III antiarrhythmic drugs block HERG, a human cardiac delayed rectifier K^+ channel - open-channel block by methanesulfonanilides. *Circulat. Res.* **78**, 499–503.
4. Franqueza, L., Longobardo, M., Vicente, J., Delpon, E., Tamkun, M. M., Tamargo, J. *et al.* (1997). Molecular determinants of stereoselective bupivacaine block of hKv1.5 channels. *Circulat. Res.* **81**, 1053–1064.
5. Nilsson, J., Madeja, M. & Arhem, P. (2003). Local anesthetic block of Kv channels: role of the S6 helix and the S5-S6 linker for bupivacaine action. *Mol. Pharmacol.* **63**, 1417–1429.
6. Mitcheson, J. S., Chen, J., Lin, M., Culberson, C. & Sanguinetti, M. C. (2000). A structural basis for drug-induced long QT syndrome. *Proc. Natl Acad. Sci. USA*, **97**, 12329–12333.
7. Zhou, M., Morais-Cabral, J. H., Mann, S. & MacKinnon, R. (2001). Potassium channel receptor site for the inactivation gate and quaternary amine inhibitors. *Nature*, **411**, 657–661.
8. Lenaeus, M. J., Vamvouka, M., Focia, P. J. & Gross, A. (2005). Structural basis of TEA blockade in a model potassium channel. *Nature Struct. Biol.* **12**, 454–459.
9. Crouzy, S., Bernèche, S. & Roux, B. (2001). Extracellular blockade of K^+ channels by TEA: results from molecular dynamics simulations of the KcsA channel. *J. Gen. Physiol.* **118**, 207–217.
10. Luzhkov, V. B., Nilsson, J., Arhem, P. & Aqvist, J. (2003). Computational modelling of the open-state K (v)1.5 ion channel block by bupivacaine. *Biochim. Biophys. Acta*, **1652**, 35–51.
11. Luzhkov, V. B., Osterberg, F. & Aqvist, J. (2003). Structure-activity relationship for extracellular block of K^+ channels by tetraalkylammonium ions. *FEBS Letters*, **554**, 159–164.
12. Ashcroft, F. M. (2002). *Ion Channels and Disease.* Academic Press, San Diego, CA.
13. Wickenden, A. D. (2002). K^+ channels as therapeutic drug targets. *Pharmacol. Ther.* **94**, 157–182.
14. Armstrong, C. M. (1971). Interaction of tetraethylammonium ion derivatives with potassium channels of giant axons. *J. Gen. Physiol.* **58**, 413–437.
15. Choi, K. L., Aldrich, R. W. & Yellen, G. (1991). Tetraethylammonium blockade distinguishes two inactivation mechanisms in voltage-activated K^+ channels. *Proc. Natl Acad. Sci. USA*, **88**, 5092–5095.
16. Mackinnon, R. & Yellen, G. (1990). Mutations affecting TEA blockade and ion permeation in voltage-activated K^+ channels. *Science*, **250**, 276–279.
17. Yellen, G., Jurman, M. E., Abramson, T. & Mackinnon, R. (1991). Mutations affecting internal TEA blockade identify the probable pore-forming region of a K^+ channel. *Science*, **251**, 939–942.
18. Holmgren, M., Smith, P. L. & Yellen, G. (1997). Trapping of organic blockers by closing of voltage-dependent K^+ channels: evidence for a trap door mechanism of activation gating. *J. Gen. Physiol.* **109**, 527–535.
19. Cuello, L. G., Romero, J. G., Cortes, D. M. & Perozo, E. (1998). pH-dependent gating in the Streptomyces lividans K+ channel. *Biochemistry*, **37**, 3229–3236.
20. Heginbotham, L., Kolmakova-Partensky, L. & Miller, C. (1998). Functional reconstitution of a prokaryotic K^+ channel. *J. Gen. Physiol.* **111**, 741–749.
21. Doyle, D. A., Cabral, J. M., Pfuetzner, R. A., Kuo, A. L., Gulbis, J. M., Cohen, S. L. *et al.* (1998). The structure of the potassium channel: molecular basis of K^+ conduction and selectivity. *Science*, **280**, 69–77.
22. Zhou, Y. F., Morais-Cabral, J. H., Kaufman, A. & MacKinnon, R. (2001). Chemistry of ion coordination and hydration revealed by a K^+ channel-Fab complex at 2.0 angstrom resolution. *Nature*, **414**, 43–48.
23. Cordero-Morales, J. F., Cuello, L. G., Zhao, Y. X., Jogini, V., Cortes, D. M., Roux, B. & Perozo, E. (2006). Molecular determinants of gating at the potassium-channel selectivity filter. *Nature Struct. Mol. Biol.* **13**, 311–318.
24. Bernèche, S. & Roux, B. (2001). Energetics of ion conduction through the K^+ channel. *Nature*, **414**, 73–77.
25. Noskov, S. Y., Bernèche, S. & Roux, B. (2004). Control of ion selectivity in potassium channels by electrostatic and dynamic properties of carbonyl ligands. *Nature*, **431**, 830–834.
26. Aqvist, J. & Luzhkov, V. (2000). Ion permeation mechanism of the potassium channel. *Nature*, **404**, 881–884.
27. Shrivastava, I. H. & Sansom, M. S. P. (2000). Simulations of ion permeation through a potassium channel: molecular dynamics of KcsA in a phospholipid bilayer. *Biophys. J.* **78**, 557–570.
28. Shrivastava, I. H., Tieleman, D. P., Biggin, P. C. & Sansom, M. S. P. (2002). K^+ versus Na^+ ions in a K channel selectivity filter: a simulation study. *Biophys. J.* **83**, 633–645.
29. MacKinnon, R., Cohen, S. L., Kuo, A. L., Lee, A. & Chait, B. T. (1998). Structural conservation in prokaryotic and eukaryotic potassium channels. *Science*, **280**, 106–109.
30. Lu, Z., Klem, A. M. & Ramu, Y. (2001). Ion conduction pore is conserved among potassium channels. *Nature*, **413**, 809–813.
31. Kutluay, E., Roux, B. & Heginbotham, L. (2004). Probing the mechanism of internal TEA block of KcsA. *Biophys. J.* **86**, 130A–131A.
32. Gao, L., Mi, X., Paajanen, V., Wang, K. & Fan, Z. (2005). Activation-coupled inactivation in the bacterial potassium channel KcsA. *Proc. Natl Acad. Sci. USA*, **102**, 17630–17635.
33. Schrempf, H., Schmidt, O., Kummerlen, R., Hinnah, S., Muller, D., Betzler, M. *et al.* (1995). A prokaryotic potassium ion channel with two predicted transmembrane segments from Streptomyces lividans. *EMBO J.* **14**, 5170–5178.
34. Heginbotham, L., LeMasurier, M., Kolmakova-Partensky, L. & Miller, C. (1999). Single streptomyces lividans K(+) channels: functional asymmetries and sidedness of proton activation. *J. Gen. Physiol.* **114**, 551–560.
35. Irizarry, S. N., Kutluay, E., Drews, G., Hart, S. J. & Heginbotham, L. (2002). Opening the KcsA K^+ channel: tryptophan scanning and complementation

analysis lead to mutants with altered gating. *Biochemistry*, **41**, 13653–13662.
36. LeMasurier, M., Heginbotham, L. & Miller, C. (2001). KcsA: it's a potassium channel. *J. Gen. Physiol.* **118**, 303–314.
37. Morais-Cabral, J. H., Zhou, Y. & MacKinnon, R. (2001). Energetic optimization of ion conduction rate by the K^+ selectivity filter. *Nature*, **414**, 37–42.
38. Swenson, R. P. J. & Armstrong, C. M. (1981). K^+ channels close more slowly in the presence of external K^+ and Rb^+. *Nature*, **291**, 427–429.
39. Ray, E. C. & Deutsch, C. (2006). A trapped intracellular cation modulates K^+ channel recovery from slow inactivation. *J. Gen. Physiol.*, **128**.
40. Jogini, V. & Roux, B. (2005). Electrostatics of the intracellular vestibule of K^+ channels. *J. Mol. Biol.* **354**, 272–288.
41. Heginbotham, L. & Kutluay, E. (2004). Revisiting voltage-dependent relief of block in ion channels: a mechanism independent of punchthrough. *Biophys. J.* **86**, 3663–3670.
42. Krantz, B. A., Melnyk, R. A., Zhang, S., Juris, S. J., Lacy, D. B., Wu, Z. Y. *et al.* (2005). A phenylalanine clamp catalyzes protein translocation through the anthrax toxin pore. *Science*, **309**, 777–781.
43. Luzhkov, V. B., Osterberg, F., Acharya, P., Chattopadhyaya, J. & Aqvist, J. (2002). Computational and NMR study of quaternary ammonium ion conformations in solution. *Phys. Chem. Chem. Phys.* **4**, 4640–4647.
44. Faraldo-Gómez, J. D. & Roux, B. (2006). Characterization of conformational equilibria through Hamiltonian and temperature replica-exchange simulations: assessing entropic and environmental effects. *J. Comput. Chem.* In the press.
45. Villaroel, A., Alvarez, O., Oberhauser, A. & Latorre, R. (1988). Probing a Ca^{2+} activated K^+ channel with quaternary ammonium ions. *Plufgers Arch.* **413**, 118–126.
46. Choi, K. L., Mossman, C., Aube, J. & Yellen, G. (1993). The internal quaternary ammonium receptor-site of Shaker potassium channels. *Neuron*, **10**, 533–541.
47. French, R. J. & Shoukimas, J. J. (1981). Blockage of squid axon potassium conductance by internal tetra-N-alkylammonium ions of various sizes. *Biophys. J.* **34**, 271–291.
48. Guo, D. L. & Lu, Z. (2001). Kinetics of inward-rectifier K^+ channel block by quaternary alkylammonium ions: dimension and properties of the inner pore. *J. Gen. Physiol.* **117**, 395–405.
49. Colquhoun, D. & Sigworth, F. J. (1995). Fitting and statistical analysis of single-channel records. In *Single Channel Recordings* (Sakmann, B. & Neher, E., eds), pp. 483–587, Plenum Press, New York.
50. Woodhull, A. M. (1973). Ionic blockage of sodium channels in nerve. *J. Gen. Physiol.* **61**, 687–708.
51. Otwinowski, Z. & Minor, W. (1997). Processing of X-ray diffraction data collected in oscillation mode. In *Methods in Enzymology Macromolecular Crystallography, Pt. A.* (Carter, C. W., Jr. & Sweet, R. M., eds), vol. 276, pp. 307–326, Academic Press, New York, London.
52. Brunger, A. T., Adams, P. D., Clore, G. M., DeLano, W. L., Gros, P., Grosse-Kunstleve, R. W. *et al.* (1998). Crystallography and NMR system: a new software suite for macromolecular structure determination. *Acta Crystallog. sect. D*, **54**, 905–921.
53. Woo, H. J., Dinner, A. R. & Roux, B. (2004). Grand canonical Monte Carlo simulations of water in protein environments. *J. Chem. Phys.* **121**, 6392–6400.
54. Im, W., Bernèche, S. & Roux, B. (2001). Generalized solvent boundary potential for computer simulations. *J. Chem. Phys.* **114**, 2924–2937.
55. Sugita, Y. & Okamoto, Y. (2000). Replica-exchange multicanonical algorithm and multicanonical replica-exchange method for simulating systems with rough energy landscape. *Chem. Phys. Letters*, **329**, 261–270.
56. Fukunishi, H., Watanabe, O. & Takada, S. (2002). On the Hamiltonian replica exchange method for efficient sampling of biomolecular systems: application to protein structure prediction. *J. Chem. Phys.* **116**, 9058–9067.
57. Brooks, B. R., Bruccoleri, R. E., Olafson, B. D., States, D. J., Swaminathan, S. & Karplus, M. (1983). CHARMM—A program for macromolecular energy, minimization, and dynamics calculations. *J. Comput. Chem.* **4**, 187–217.
58. MacKerell, A. D., Bashford, D., Bellott, M., Dunbrack, R. L., Evanseck, J. D., Field, M. J. *et al.* (1998). All-atom empirical potential for molecular modeling and dynamics studies of proteins. *J. Phys. Chem. B*, **102**, 3586–3616.

Edited by J. Bowie

(Received 7 July 2006; received in revised form 22 September 2006; accepted 24 September 2006)
Available online 29 September 2006